Control of Cytoskeletal Mechanics by Extracellular Matrix, Cell Shape, and Mechanical Tension

Ning Wang* and Donald E. Ingber‡
*Physiology Program, Department of Environmental Health, Harvard School of Public Health, and ‡Departments of Surgery and Pathology, Children's Hospital and Harvard Medical School, Boston, Massachussetts 02115 USA

ABSTRACT We have investigated how extracellular matrix (ECM) alters the mechanical properties of the cytoskeleton (CSK). Mechanical stresses were applied to integrin receptors on the apical surfaces of adherent endothelial cells using RGD-coated ferromagnetic microbeads (5.5-μm diameter) in conjunction with a magnetic twisting device. Increasing the number of basal cell-ECM contacts by raising the fibronectin (FN) coating density from 10 to 500 ng/cm^2 promoted cell spreading by fivefold and increased CSK stiffness, apparent viscosity, and permanent deformation all by more than twofold, as measured in response to maximal stress (40 dyne/cm^2). When the applied stress was increased from 7 to 40 dyne/cm^2, the stiffness and apparent viscosity of the CSK increased in parallel, although cell shape, ECM contacts, nor permanent deformation was altered. Application of the same stresses over a lower number ECM contacts using smaller beads (1.4-μm diameter) resulted in decreased CSK stiffness and apparent viscosity, confirming that this technique probes into the depth of the CSK and not just the cortical membrane. When magnetic measurements were carried out using cells whose membranes were disrupted and ATP stores depleted using saponin, CSK stiffness and apparent viscosity were found to rise by approximately 20%, whereas permanent deformation decreased by more than half. Addition of ATP (250 μM) under conditions that promote CSK tension generation in membrane-permeabilized cells resulted in decreases in CSK stiffness and apparent viscosity that could be detected within 2 min after ATP addition, before any measurable change in cell size. Permanent deformation only decreased after 20 min, once the CSK lattice had physically contracted. Importantly, regardless of cell shape or membrane continuity, CSK stiffness increased in direct proportion to the applied stress, as predicted by tensegrity (tensional integrity) cell models. These results suggest that the effects of ECM on CSK mechanics are not due to changes in osmotic or hydrostatic pressures. Rather, ECM alters CSK stiffness and apparent viscosity by binding integrins, promoting formation of molecular links with the CSK, transmitting mechanical stresses across these linkages, and inducing structural rearrangements within a continuous, tensionally integrated CSK lattice. In contrast, permanent deformation in the CSK appears to be more tightly coupled to cell extension and depends on both passive plasticity and dynamic remodeling events.

INTRODUCTION

Control of cell shape by extracellular matrix (ECM) is critical for regulation of cell growth (Folkman and Moscona, 1978; Ingber, 1990), differentiation (Bissell et al., 1982; Mooney et al., 1992), cell polarity (Ingber et al., 1986), and tissue pattern (Emerman and Pitelka, 1977; Ingber et al., 1981; Ingber and Folkman, 1989). ECM regulates cell and tissue morphogenesis by altering the structure of the intracellular cytoskeleton (CSK) which, in turn, serves to orient much of the cell's metabolic machinery (Ingber, 1993a). Although many studies have focused on the molecular basis of CSK polymerization and assembly (reviewed in Stossel, 1993), little is known about the role of CSK mechanics in cell shape determination. Mechanical properties of cell surfaces have been measured with micropipette aspiration (reviewed by Hochmuth and Waugh, 1987; Evans and Yeung, 1989) and cell poker techniques (Peterson et al., 1982). Intracellular viscoelasticity and motility also have been quantitated using cell magnetometry (Valberg, 1984; Valberg and Albertini, 1985; Valberg and Feldman, 1987; Bizal et al., 1991). However, all of these approaches are based on nonspecific deformation of a large portion of the cell, and thus, none of these methods permits direct probing of specific molecular structures within the CSK. Furthermore, the mechanism of ECM-dependent shape control has not been the focus of study using any of these techniques.

We recently described a magnetic twisting device (Wang et al., 1993) in which controlled mechanical stresses can be applied directly to cell surface ECM receptors (integrins) and, hence, the CSK, using ferromagnetic microbeads that are coated with specific integrin ligands, such as RGD (Arg-Gly-Asp)-containing peptides. The cellular response to applied stress is simultaneously measured by quantitating changes in the rotation (angular strain) of the surface-bound magnetic beads using a sensitive in-line magnetometer. In the present study, we used this magnetic twisting device to quantitate effects on CSK mechanics that result from independently varying cell-ECM contacts, cell shape, applied mechanical stresses, and the area over which forces are applied. Studies were also carried out with membrane-permeabilized cells to discriminate between osmotic and CSK effects on cell responses as well as static versus dynamic changes in the CSK.

Received for publication 4 November 1993 and in final form 30 March 1994.
Address reprint requests to Dr. Donald Ingber, Enders 1007, Children's Hospital, 300 Longwood Ave., Boston, MA 02115. Tel.: 617-735-8031; Fax: 617-232-7914.

0006-3495/94/06/2181/09 $2.00

MATERIALS AND METHODS

Bovine capillary endothelial cells were cultured to confluence, serum-deprived, trypsinized, and plated in defined medium on 96-well plates (Removawells, Immulon II, Dynatech, Chantilly VA) that were coated with human serum fibronectin (FN; Cappel) as previously described (Ingber, 1990). The shape of adherent cells was varied from round to spread by increasing the FN coating density from 10 to 500 ng/cm^2. Projected areas of adherent cells were determined using a computer image analysis system (Ingber, 1990). A total of 45 cells within five randomly selected areas from three different culture wells were measured for each cell area determination.

In studies analyzing the role of membrane integrity, cells were made permeable with saponin as previously described (Sims et al., 1992). In brief, cells cultured for 3 h on high FN were washed once in a CSK stabilization buffer (50 mM KCl, 10 mM imidazole, 1 mM EGTA, 1 mM $MgSO_4$, 0.5 mM dithiothreitol, 5 μg/ml aprotinin, 5 μg/ml leupeptin, 0.1 mM PMSF, and 20 mM PIPES, pH 6.5) that preserves contractile microfilaments in a functional form. Cells were then incubated in the same buffer containing saponin (25 μg/ml; Sigma Chemical Co., St. Louis, MO) for 10 min at 37°C and were induced to retract by addition of 250 μM ATP in a tension-generation buffer (250 μM $CaCl_2$, 50 mM KCl, 1 mM EGTA, 2 mM $MgSO_4$, 0.5 mM dithiothreitol, 5 μg/ml aprotinin, 5 μg/ml leupeptin, 0.1 mM PMSF, 2 M glycerol, and 25 mM PIPES, pH 7.0).

CSK mechanics were quantitated in intact and membrane-permeabilized cells using a magnetic twisting device in which controlled mechanical loads are applied directly to apical cell surface receptors without producing a global cell shape change (Wang et al., 1993). In brief, cells adherent to FN-coated wells for 3–10 h were allowed to bind to spherical ferromagnetic beads (5.5 or 1.4 μm diameter) that were precoated with a synthetic RGD-containing peptide (Peptite 2000; Telios), which is a specific ligand for integrin receptors. After 10–20 min, unbound beads were washed away with 1% BSA/DMEM and the wells were individually placed into the magnetic twisting device and maintained at 37°C. A brief (10 μs) but strong (1000 gauss) homogeneous magnetic pulse was then applied to magnetize all surface-bound beads in the horizontal direction. After 20 s, a twisting torque was produced by applying a weaker magnetic field (0–25 gauss) in the vertical direction for 1 min. Because this field was small, it did not realign the bead magnetic moments; rather, it rotated beads in place in the same direction.

The extent of bead rotation was measured by an in-line magnetometer that continuously detected the magnitude of the bead magnetic vector in the horizontal direction. The torque of the applied twisting field was proportional to the twisting field, bead magnetization, and the sine of the angle between the twisting field vector and the bead magnetization vector (see Appendix). The resulting shear stress was transmitted to the cell through bead-integrin interactions causing the intracellular CSK to deform without producing large-scale changes in cell shape (Wang et al., 1993). The twisting field was then turned off for 1 min, and the extent of recovery of the bead magnetic signal after twisting, a measure of the energy stored elastically in the cell, was quantitated. Applied stress, angular strain, apparent viscosity, permanent deformation (percent angular strain sustained after applied stress was released), and stiffness were determined as described in the Appendix. Apparent stiffness was defined as the ratio of stress to strain (i.e., rather than the derivative of stress with respect to strain). Control experiments demonstrating the specificity of force transfer across integrins have been published previously (Wang et al., 1993). These studies include demonstration that force transfer by RGD-beads can be inhibited using soluble GRGDSP peptide but not GRGESP; beads coated with antibodies directed against specific integrin subunits produce similar effects; and that beads coated with ligands for nonadhesion receptors (e.g., acetyl-LDL receptors) fail to produce an effective CSK response.

RESULTS

Studies were carried out to determine the effects of independently varying ECM contacts, cell shape, and mechanical tension on CSK mechanics. Increasing the FN density from low to high (10 to 500 ng/cm^2) promoted cell spreading and resulted in a fivefold increase in projected cell areas (from 350 to 1640 μm^2) when measured 6 h after plating (Fig. 1). Assuming cell volume did not change, cell heights under these conditions were estimated as approximately 3–4 μm for spread cells and 15–16 μm for round cells given these projected areas and the diameter of the cells when round and in suspension (20 μm). These values fit nicely with those from past studies with cultured endothelial cells in which cell heights were measured directly (Folkman and Moscona, 1978; Barbee et al., 1994). When RGD-coated magnetic microbeads were added to these cells, greater than 95% bound over the cell body with less than 5% over lamellopodia or long thin cell extensions.

Cells that were prevented from spreading and those that were fully extended both exhibited nonlinear stress-strain relationships when the bound microbeads were magnetically twisted (Fig. 2 *A*). However, greater angular strains were observed in response to the same applied stresses (0–40 dyne/cm^2) in round cells on low FN when compared with spread cells on high. Stress-induced stiffening was also observed in cells on both FN densities, but the stiffening response (slope

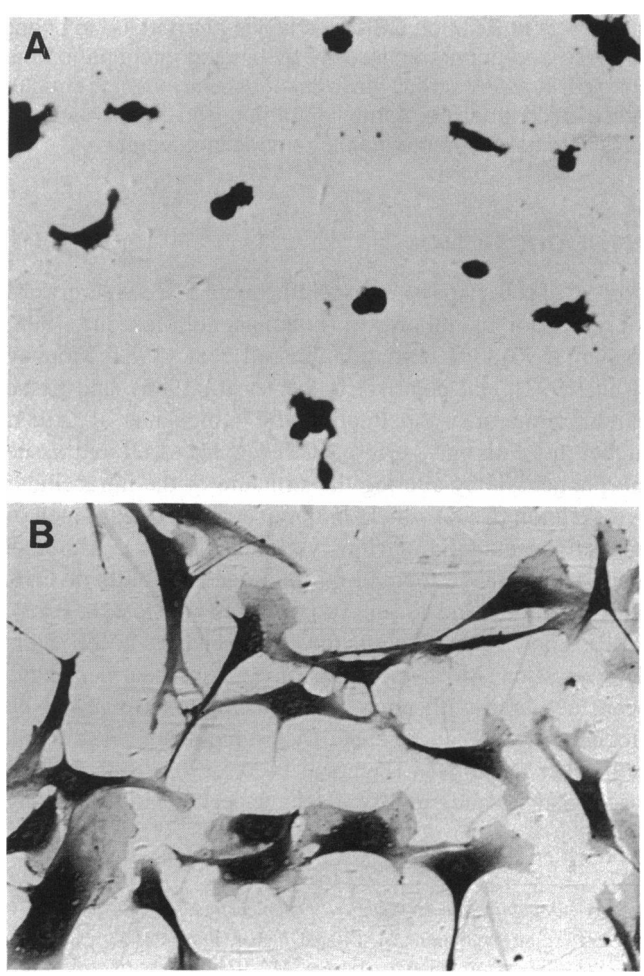

FIGURE 1 Control of endothelial cell shape by FN. Cells were plated for 6 h on dishes coated with FN at 10 (*A*) or 500 (*B*) ng/cm^2 and stained with Coomassie Brilliant blue. (×320).

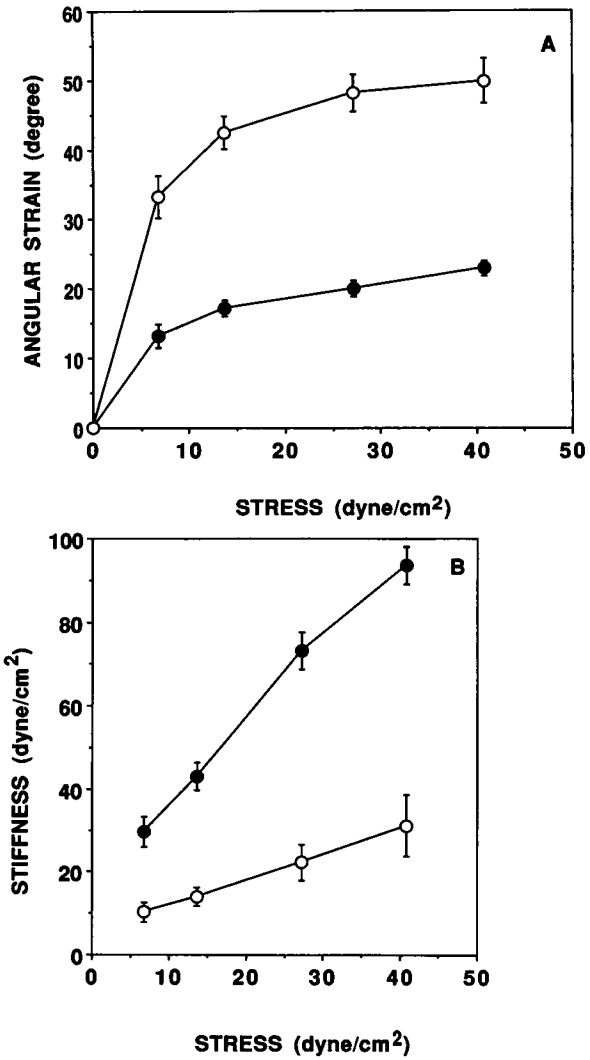

FIGURE 2 Measurements of angular strain (*A*) and stiffness (*B*) obtained by applying mechanical stresses to integrins of endothelial cells cultured on different FN densities using the magnetic twisting device. Note that the stress-strain relationships are nonlinear for both round cells and spread cells and, hence, the stiffening response is linear under both conditions. In this experiment in which 5.5-μm-diameter beads were utilized, stress was converted from torque as: 1 dyne/cm^2 stress = 5.2 μdyne μm. Stiffness was defined as the ratio of stress to strain. (○) Round cells on low FN (10 ng/cm^2); (●) spread cells cells on high FN (500 ng/cm^2). Error bars = SEM; n = 3.

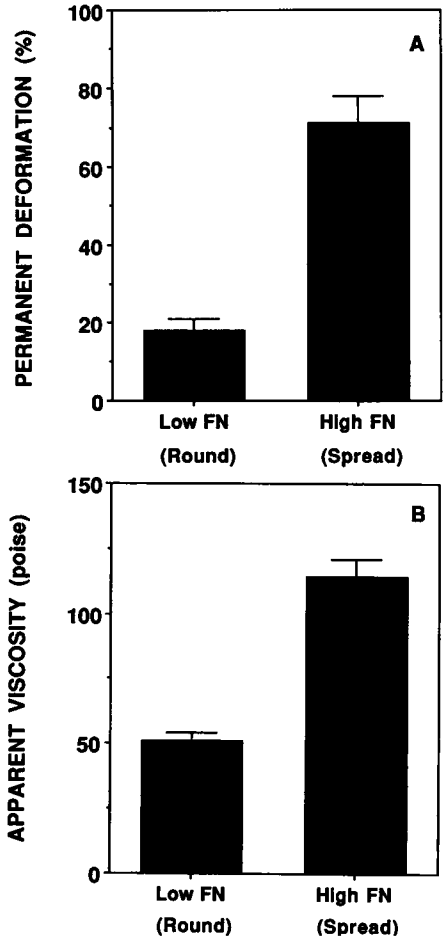

FIGURE 3 Measurements of Permanent Deformation (*A*) and Apparent Viscosity (*B*) of endothelial cells cultured on different FN densities. (*A*) The percent deformation retained after applied stress (40 dyne/cm^2) was released was significantly higher in spread cells on high FN versus round cells on low. (*B*) Apparent viscosity was also greater in spread cells on high FN.

of stiffness versus stress) of the well extended cells was approximately 3 times that displayed by round cells (1.9 vs. 0.6, curve fitting R^2 = 0.99) (Fig. 2 *B*). The permanent deformation (Fig. 3 *A*) and apparent viscosity (Fig. 3 *B*) of the CSK were also about 2–3 times higher in spread cells compared to round. It should be noted that the absolute values for applied stresses that are presented are only approximations because the beads are only partly embedded in the cells when the magnetic measurements are carried out (see Fig. 3 in Wang et al., 1993). However, studies in which the response to the same applied stress has been measured over time have revealed that angular strain only decreases by about 30% from 15 min to 2 h after bead addition (i.e., over the time in which complete bead engulfment occurs). Thus, use of total bead surface area for our calculations appears to be a reasonable approximation.

To confirm that the surface-bound magnetic beads were probing three-dimensional (3D) structures within the CSK lattice, rather than the membrane or cortical CSK alone, the cell surface area over which forces were applied was varied while maintaining the mechanical stresses constant. Beads with different diameters (d = 5.5 vs. 1.4 μm) were used for this purpose. For a 3D elastic structure, the apparent stress as a function of strain will be invariant with bead diameter, whereas for a two dimensional (2D) structure, stress is inversely proportional to diameter at each value of strain. The results in Fig. 4 *A* show that at given values of strain, stress for the larger bead was systematically larger than for the smaller bead. This result is the exact opposite of what would be predicted if a 2D medium were the source of elastic forces. Inspection of Fig. 4 *B* also shows that, at least for small stresses and strains, apparent stiffness (stress/strain) versus stress changes little with bead diameter (i.e., the intersection with the stress = 0 axis is similar for both sized beads),

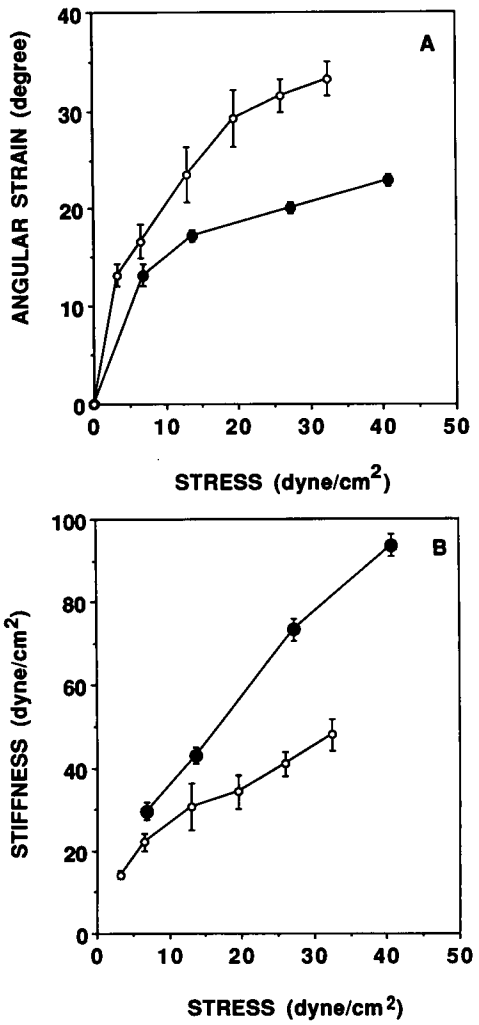

FIGURE 4 Measurements of angular strain (*A*) and stiffness (*B*) within spread cells on high FN obtained by applying mechanical stresses using different sized beads. Varying the surface area over which forces were applied altered angular strain and stiffness, although cell shape was not altered. In studies in which 1.4-μm beads were utilized, stress was converted from torque as: 1 dyne/cm^2 stress = 0.086 μdyne μm. (○) 1.4-μm-diameter beads; (●) 5.5-μm-diameter beads.

consistent with the notion that we are probing a 3D medium. However, the observed change of stress with bead diameter at large strains suggests that the initial assumption of the CSK as an infinite 3D medium may be an oversimplification. Furthermore, the observed divergence for different sized beads at large deformations is in the correct direction for cell boundary effects, which we would expect to be particularly prominent in spread cells whose thickness (3–4 μm) was less than the diameter of the large beads. The importance of boundary effects is further supported by the finding that the slope of stiffness scaled directly with the ratio of bead size to cell height and inversely with the ratio of bead size to cell area in round versus spread cells (Fig. 2 *B*). Apparent viscosity was also approximately 50% lower when measured with smaller beads at higher applied stresses; however, no significant difference in permanent deformation was observed under these conditions in which cell shape was held constant (data not shown).

As described above, when we extrapolated the stiffness values that we obtained to zero applied stress (a measure of endogenous CSK mechanical properties), we found that this intercept was nearly identical for cells of the same shape, but measured with different sized beads (Fig. 4 *B*). In contrast, when cells with different shapes were analyzed, stiffness at zero applied stress changed significantly (6 dyne/cm^2 in round cells compared with 17 dyne/cm^2 in spread; Fig. 2 *B*). Calculation of stiffness at zero applied stress, therefore, may provide a simple way to quantitate changes in the mechanical properties of the CSK that accompany cell shape changes.

To discriminate between active (ATP-dependent) and passive (ATP-independent) properties of the CSK and between osmotic and CSK effects, cell membranes were made permeable with the detergent saponin. The resulting loss of membrane continuity and depletion of cytoplasmic ATP resulted in approximately a 15–20% increase in both CSK stiffness (Fig. 5 *A*) and apparent viscosity (Fig. 5 *B*); in contrast, permanent deformation decreased by more than half (Fig. 5 *C*). Addition of ATP (250 μM) to saponin-permeabilized endothelial cells results in CSK tension generation and causes cells to retract progressively from their basal FN contacts, although membrane continuity is lost (Sims et al., 1992). Addition of the same concentration of ATP resulted in rapid and progressive decreases in CSK stiffness (Fig. 5 *A*) and apparent viscosity (Fig. 5 *B*), which were apparent within 2 min after ATP addition, before any measurable change in cell size. A small, but significant, decrease in permanent deformation was first observed after only 20 min of ATP addition, when the CSK lattice physically retracted; there was no change in permanent deformation at early times (Fig. 5 *C*). Interestingly, although both transmembrane osmotic pressure differences and membrane continuity were lost, CSK stiffness still increased in direct proportion as the level of applied stress was raised (data not shown), as previously observed in intact cells (Fig. 2 *B*).

DISCUSSION

To understand how ECM controls cell shape and function, we must first define the mechanism by which adhesion to ECM induces changes in CSK architecture. Alterations in the form of the CSK involve both biochemical polymerization events (Stossel, 1993) and mechanically induced changes in CSK filament distribution and pattern (Ingber, 1993b). Although much information has been gathered about the molecular basis of CSK filament assembly, little is known about the biophysical mechanism by which mechanical stresses produce changes in CSK structure. This is an important point because cell shape and associated functions are normally controlled as a result of mechanical interactions between cells and their ECM attachment substrate. In general, cells spread and grow on rigid ECM, but they retract, round, and differentiate on malleable foundations (reviewed in Ingber, 1991). It is essential, therefore, to understand how changing

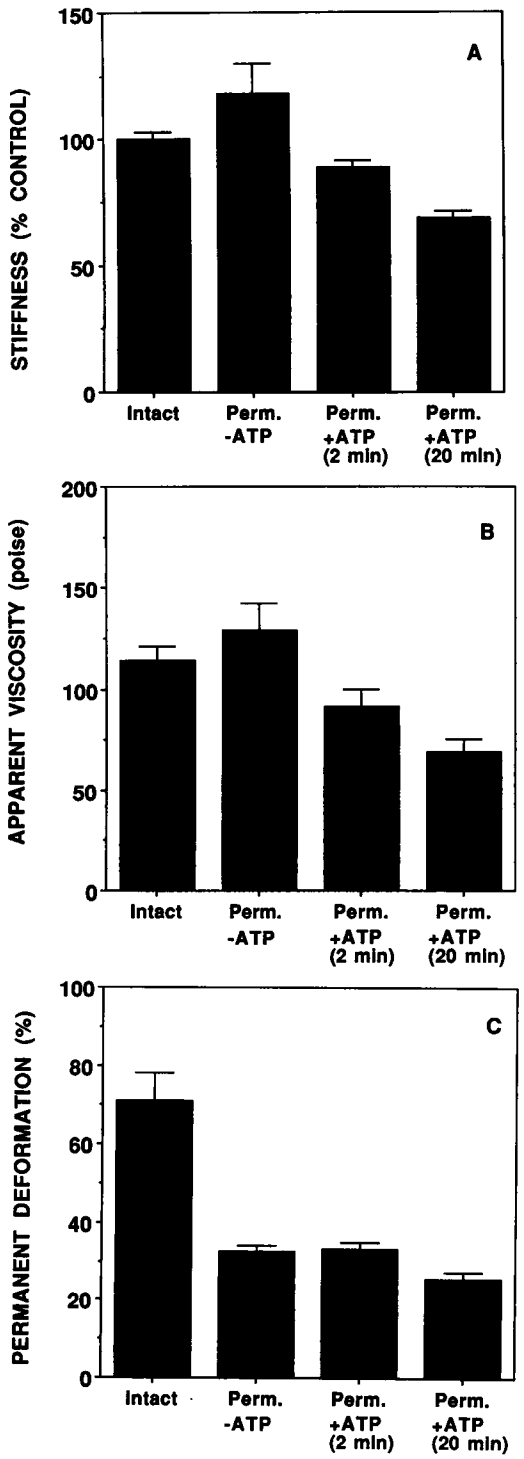

FIGURE 5 Stiffness (*A*), Apparent Viscosity (*B*), and Permanent Deformation (*C*) of cells on high FN before and after membrane permeabilization and addition of ATP (250 μM). Cells were plated for 3 h before mechanical measurements were carried out. Measurements were carried out with: intact cells before permeabilization (Intact), cells permeabilized with saponin and incubated in buffer without ATP (Perm. – ATP), and cells permeabilized with saponin and incubated in buffer with ATP for 2 or 20 min (Perm. + ATP 2 min or 20 min, respectively). Baseline stiffness of intact cells was 57 ± 3 dyne/cm^2.

the balance of mechanical forces that are transferred across the cell's adhesion sites alters CSK structure.

In the present study, we utilized a magnetic twisting device (Wang et al., 1993) to apply controlled mechanical stresses to cells and simultaneously to measure a CSK response. Past methods used to analyze cell mechanics relied on nonspecific deformation of large regions of the cell surface (e.g., cell poking) and thus, the amount of force transmitted to the CSK depended largely on the degree of membrane deformation (Peterson et al., 1982). Furthermore, the path by which force was transferred across the cell surface was likely not the same as that which is normally utilized in living cells. In contrast, our magnetic manipulation approach permits us to apply forces directly to transmembrane integrin receptors that physically interlink ECM with the CSK without producing large-scale changes in cell shape. In the present study, we used this technique to explore the roles of ECM, cell shape, mechanical tension, and plasma membrane integrity in the control of CSK mechanics.

Our results show that the mechanical properties of the CSK (i.e., stiffness, permanent deformation, and apparent viscosity) are sensitive to changes in all of these variables. Varying cell shape from round to spread, by increasing the density of ECM contacts at the cell base, increased CSK stiffness, permanent deformation, and apparent viscosity (measured at the cell apex) by more than twofold. In contrast, increasing ECM contacts independently of cell shape, by allowing cells to bind to different sized beads, increased only CSK stiffness and apparent viscosity; permanent deformation was not altered. Stiffness and viscosity also changed without affecting permanent deformation when we increased the mechanical stress applied over a single sized bead and, hence, over a constant number of ECM contacts. Thus, these data indicate that ligating integrins or changing the mechanical stresses that are transferred across these ECM receptors is sufficient to alter the stiffness and viscosity of the entire CSK. In contrast, permanent deformation, the ability of the cell to sustain structural alterations, appears to scale more closely with cell shape.

Furthermore, using membrane-permeabilized cells, we were able to demonstrate that the CSK, rather than intracellular osmotic or hydrostatic pressures (Oster, 1984), is the major determinant of cell shape and mechanics. Importantly, in both intact and membrane-permeabilized cells, repetitive application of the same stress resulted in nearly identical permanent deformation, suggesting that there was little, if any, damage inflicted on the CSK in the range of stresses we applied. Our studies with different sized beads also confirmed that the magnetic twisting method probes into the depth of the CSK and does not simply measure properties of the cell cortex. However, our data also demonstrate that the living CSK does not behave as an infinite, isotropic 3D structure. Thus, new models will be necessary to understand better the mechanical behavior of living cells.

All of the cells we studied, regardless of shape or membrane integrity, exhibited linear CSK stiffening behavior:

stiffness increased in direct proportion to the level of applied stress. Although this type of mechanical behavior is observed in many biological tissues, it cannot be explained by conventional biomechanical theories (McMahon, 1984; Stamenovic, 1990). This response to stress could be due to global structural rearrangements with the CSK. For example, we have recently shown that this linear stiffening response can be explained if the CSK is a tensionally integrated (tensegrity) structure, that is, a molecular continuum of mechanically interdependent struts and tensile elements that rearrange globally, rather than deform locally, in response to stress (Wang et al., 1993; Ingber, 1993b). If the CSK acts as if it were a tensegrity structure, then its ability to resist angular deformation and, hence, its "stiffness," would not be a function of the deformability of individual filaments; rather, it would be a property of the integrated CSK lattice.

The enhanced stiffness observed within the CSK of extended cells on high FN may be due to increased focal adhesion formation, elevated CSK stresses associated with isometric tension generation (stress is dissipated when cells retract), and resultant local realignment of filaments within the continuous CSK lattice (e.g., stress fiber formation; Ingber, 1993b). In support of this possibility, stiffness also decreased when membrane-permeabilized cells were induced to detach physically from their ECM adhesions by addition of ATP. Stress fibers also dissociate when these saponin-permeabilized cells retract (Sims et al., 1992). However, the findings that disruption of membrane integrity and concomitant loss of ATP resulted in a rapid increase in CSK stiffness (Fig. 5 *A*) and that readdition of ATP immediately reversed this effect imply that the rigidity of the CSK also depend on ATP-dependent molecular transformations, such as actomyosin filament sliding (e.g., *rigor mortis* would be observed in the absence of ATP) or chemical modification of CSK proteins (e.g., phosphorylation).

Apparent viscosity of the CSK is a function of the energy dissipation that results when the CSK lattice is deformed. CSK stiffness and apparent viscosity normally change in parallel in cells because alterations in CSK filament alignment that are induced by cell binding to ECM, application of mechanical stresses, or cell extension likely result in increased interfilamental friction and, thus, enhanced energy dissipation. Interestingly, the value for apparent viscosity we measured in spread endothelial cells was about 150 poise, which is an order of magnitude lower than that previously reported for adherent macrophages using the same cell magnetometry system in combination with engulfed magnetic particles (approximately 2000 poise; Bizal et al., 1991; also reviewed in Valberg and Feldman, 1987). In these past studies, elastic retarding torque (see Appendix) was ignored when viscosity was calculated, resulting in about a four- to fivefold overestimation of apparent viscosity. The remainder of this difference in apparent viscosity may be because mechanical stresses were applied directly to molecules (integrins) that are mechanically coupled to the CSK in the present study, whereas nonspecific methods of deformation (i.e., twisting uncoated ferromagnetic fibrils constrained within intracellular lysosomes) were used in the past.

In contrast with CSK stiffness and viscosity, our experiments comparing intact and membrane-permeabilized cells suggest that once the applied stress is released, passive material plasticity and molecular remodeling events are primarily responsible for maintaining permanent deformation. ATP-dependent events, such as actomyosin filament sliding, did not appear to play a critical role. For example, although loss of ATP and small soluble cytoplasmic molecules due to saponin treatment decreased permanent deformation by twofold, readdition of ATP had no immediate effect. However, permanent deformation did change (decrease) as a result of actomyosin-dependent cell retraction and associated dissociation of actin filament bundles (Sims et al., 1992). Conversely, cell spreading may increase permanent deformation by producing large-scale changes in CSK architecture and thereby altering the static mechanical properties of the CSK lattice. In addition, cell extension increases structural interactions (overlap) between adjacent CSK filaments (Ingber, 1993b) and apparently promotes chemical remodeling events that serve to stabilize new molecular configurations within the CSK lattice that form in response to stress. Chemical remodeling likely involves detaching and reannealing processes within the CSK, due to the actions of various small CSK severing, cross-linking, and bundling proteins (e.g., gelsolin, filamin; Stossel, 1993) that are lost when membrane integrity is compromised.

It is important to emphasize that mechanical signal transfer between the CSK and integrins exists before exogenous force application because all adherent cells generate mechanical forces within their contractile filaments and exert these forces on their ECM contacts (reviewed by Ingber, 1991). Thus, the mechanical force balance inherent in the cell before force application is a function of endogenous prestress in the CSK. Values extrapolated for CSK stiffness at zero applied stress may provide a measure of this internal prestress. In support of this possibility, we found that applying stresses over different sized beads changed the stiffening response, but not the stiffness, at zero applied stress, whereas this measurement did change when cell shape was altered. Thus, determination of stiffness at zero applied stress could provide a simple and rapid way to estimate CSK prestress under different experimental conditions. If this is correct, then our data suggest that altering the global architecture of the cell (i.e., cell shape) changes its internal CSK force balance and vice versa.

Taken together, our data are consistent with a mechanism in which ECM alters CSK mechanics and changes cell shape by binding to transmembrane integrin receptors, inducing molecular bridge formation with the CSK, and transmitting mechanical stresses across these linkages. Resulting stress-induced structural rearrangements within a continuous tensionally integrated CSK lattice cause the stiffness and apparent viscosity of the CSK to change. In contrast, the ability of the CSK to sustain stress-induced changes in structure (permanent deformation) appears to be based primarily on

active molecular remodeling events and, to a lesser degree, on static changes in CSK structure. Importantly, the magnetic probe described in this study provides an effective way to quantitate these changes and, hence, it may be very useful for analyzing the relation between CSK mechanics, cell shape, and cell function in the future.

We thank Dr. J. P. Butler for his advice and his critical review of the Appendix, Drs. W. Moller and W. Stahlhofen for providing the ferromagnetic microbeads, J. Sims and Z. Sun for technical assistance, Drs. J. J. Fredberg and D. Stamenovic for useful discussion, and Drs. J. Brain and J. Folkman for their continued support.
This work was supported by National Institutes of Health grants HL-33009 and CA-45548 and by National Aeronautics and Space Administration grant NAG-9-430. D. Ingber is a recipient of a Faculty Research Award from American Cancer Society.

APPENDIX

This section summarizes and defines the relationships among the various biophysical parameters involved in cell magnetometry. The notation and derivations follow Valberg and Butler (1987).

Applied magnetic torque

The applied magnetic torque is given by

$$\vec{T}_{mag} = \mu_0 \vec{M} \vec{H}_a,$$

where μ_0 is permeability of free space and $\vec{M}$ = microbead magnetic moment, and $\vec{H}_a$ = external twisting field.
In scalar form, the vector cross product above becomes

$$T_{mag} = \mu_0 M H_a \sin\theta,$$

where θ is the angle between vector $\vec{M}$ and vector $\vec{H}_a$. T_{mag}, M, and H_a are the magnitude of T_{mag}, M, and H_a. Note that T_{mag} and θ will in general be functional of time t.

Viscous and elastic opposing torques

The opposing torques conferred by the material are of viscous and elastic origin, the magnitudes of which are given by
- Viscous:

$$T_{vis} = -\kappa V \eta \omega,$$

where k is a particle shape factor ($k = 6$ for a spherical microbead); V = microbead volume; η = viscosity, ω = angular velocity of the microbead rotation, and $\omega = d\theta/dt$.
- Elastic:

$$T_{elas} = \kappa V E \phi,$$

where k is the same particle shape factor as above, V = microbead volume, E = elastic modulus, ϕ = angular rotation of the microbead, $\phi = \pi/2 - \theta$. This complementary angle ϕ is used for convenience. In particular, H_a is perpendicular to M at $t = 0$; this corresponds to picking the origin of ϕ such that $\phi = 0$ at $t = 0$.

Additive torques

Neglecting inertial effects, the net torque on the microbead is zero. If we assume that the elastic and viscous contributions are mechanically in parallel, then their torques are additive and we have

$$T_{mag} = T_{vis} + T_{elas}.$$

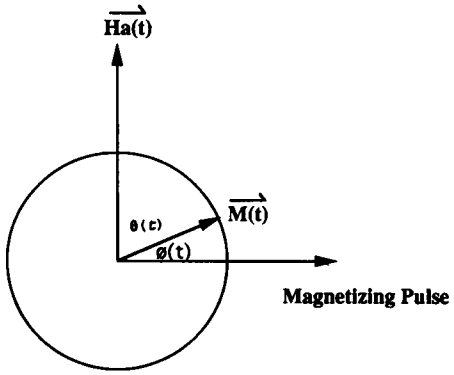

FIGURE AP1

Using the above expressions for these torques, we have

$$\mu_0 M H_a \sin\theta = -\kappa V \eta \omega + \kappa V E \phi = -\kappa V \eta \frac{d\theta}{dt} + \kappa V E (90° - \theta). \quad (1)$$

For simplicity, we have omitted contributions from active endogenous retarding torques from the cells. This equation may be used both during the field application and when the field is turned off. It should be emphasized that the linear mechanical analysis employed in the Viscous and Elastic Opposing Torques and Additive Torques sections is just an approximation, primarily useful for development of basic insights rather than quantitative parameter determination.

Measurements of angular strain from magnetic signals generated by the microbeads

The remanent magnetic field B resulting from both the amplitude M and orientation ϕ of the microbeads is measured by an in-line magnetometer. After the microbeads are magnetized by a strong horizontal pulse field (1000 gauss, 10 μs) and in the absence of the twisting field, there are only relaxation processes (Valberg and Butler, 1987; Zaner and Valberg, 1989):

$$B(t)_{relax} = B(o)\cos\phi(t)_{relax}.$$

Assuming that applying twisting fields does not change the process of relaxation, i.e., relaxation and twisting are two independent processes (Bizal et al., 1991), then we have

$$B(t)_{twist} = B(t)_{relax}\cos\phi(t).$$

We thus estimate the angular displacement of the microbead induced by the twisting field after correcting the effects of relaxation by the above two expressions:

$$\phi(t) = \cos^{-1}\left(\frac{B(t)_{twist}}{B(t)_{relax}}\right). \quad (2)$$

Calibration of applied stress (Zaner and Valberg, 1989)

Microbeads are placed in a known viscosity standard. Because there is no elastic opposing torque, from Eq. 1 we have

$$\mu_0 M H_a \sin\theta = -kV\eta \frac{d\theta}{dt}.$$

The solution of this equation for initial conditions $\theta(0) = \theta_0$ is

$$\tan(\theta/2) = \tan(\theta_0/2)e^{-t/\tau},$$

where the time constant τ is given by

$$\tau = \frac{\kappa\eta V}{\mu_0 M H_a}.$$

The logarithmic slope of $\tan(\theta/2)$ vs. t is thus $1/\tau = cH_a/\eta$. Note that cH_a has the dimension of a stress.

$$c = \frac{\mu_0 M}{\kappa V}$$

Thus, the experimental determination of $1/\tau$ from the $\theta(t)$ curve for a given H_a in a viscous standard suffices to estimate factor c. The calibration factor c is used in actual experiments to relate the observed angular displacements to the effective stress σ applied to the microbead:

$$\sigma(t) = cH_a\left(\frac{B(t)_{\text{twist}}}{B(t)_{\text{relax}}}\right). \quad (3)$$

Note that this effective stress represents the ratio of actual torque on the bead to the bead volume. We embedded the beads completely in a pure viscous fluid of 1000 poise and applied twisting field to calibrate c. Using the above method, we determined that for 5.5-μm beads, $c = 2.72$ dyne/cm^2 per gauss; for 1.4-μm beads, $c = 1.3$ dyne/cm^2 per gauss.

Stiffness

We define the stiffness, E, by a ratio analogous to a stress-strain ratio. Specifically, we write

$$E = \sigma/\phi \quad (4)$$

where σ is given by Eq. 3 and ϕ by Eq. 2. Note that this stiffness, as defined, may be a function of time. We use σ and ϕ at the end of one min twisting to calculate stiffness, and denote that quantity E_1. Note that both viscous and elastic torques may contribute to this apparent stiffness, but that when $\phi(t)$ displays an approximate plateau at $\phi = \phi_1$, then this method of estimating stiffness is primarily probing elastic features.

Calculation of permanent deformation (failure of angular recovery after the twisting field is turned off)

The magnetization pulse is applied at time 0, the twisting field is on for 1 min (from 20 s to 1 min 20 s), and is off for 1 min (from 1 min 20 s to 2 min 20 s). The induced angular strain after one min twisting is

$$\phi_1 = \cos^{-1}\left(\frac{B(\text{at 1 min 20 s})_{\text{twist}}}{B(\text{at 1 min 20 s})_{\text{relax}}}\right)$$

The angular strain remaining after the twisting field has been off for 1 min is

$$\phi_2 = \cos^{-1}\left(\frac{B(\text{at 2 min 20 s})_{\text{final}}}{B(\text{at 2 min 20 s})_{\text{relax}}}\right).$$

To the extent that ϕ_2 represents a plateau of angular recovery, the ratio ϕ_2/ϕ_1 is a measure of irreversible or permanent deformation. We thus define

$$\text{permanent deformation} = \frac{\phi_2}{\phi_1} \times 100\%. \quad (5)$$

Calculation of apparent viscosity

When the twisting field is off, from Eq. 1 we have the complementary angle ϕ:

$$0 = \kappa V\eta\frac{d\phi}{dt} + \kappa VE\phi.$$

The solution to this is

$$\phi = \phi_0 e^{-t/(\eta/E)},$$

where $\phi = \phi_0$ at $t = 0$. This function is a simple exponential decay with time constant given by the ratio of apparent viscosity to apparent stiffness. Note that this time constant is independent of both the microbead shape factor and its volume. The estimate of apparent viscosity η is then given by using the previously estimated stiffness E and this measured time constant (Butler et al., 1992).

REFERENCES

Barbee, K. A., P. F. Davies, and R. Lal. 1994. Shear stress-induced reorganization of the surface topography of living endothelial cells imaged by atomic force microscopy. *Circ. Res.* 74:163–171.

Bissell, M. J., H. G. Hall, and G. Parry. 1982. How does extracellular matrix direct gene expression? *J. Theor. Biol.* 99:31–68.

Bizal, C. L., J. P. Butler, and P. A. Valberg. 1991. Viscoelastic and motile properties of hamster lung and peritoneal macrophages. *J. Leuko. Biol.* 50:240–251.

Butler J. P., S. M. Kelly, H. Miki, R. Rogers, and P. T. Macklem. 1992. Rheology and spontaneous oscillation in *Xenopus* oocytes and eggs. *FASEB J.* 6:A1627.

Emerman, J. T., and D. R. Pitelka. 1977. Maintenance and induction of morphological differentiation in dissociated mammary epithelium on floating collagen membranes. *In Vitro* 13:316–328.

Evans, E., and A. Yeung. 1989. Apparent viscosity and cortical tension of blood granulocytes determined by micropipet aspiration. *Biophys. J.* 56: 151–160.

Folkman, J., and A. Moscona. 1978. Role of cell shape in growth control. *Nature.* 273:345–349.

Hochmuth, R. M., and R. E. Waugh. 1987. Erythrocyte membrane elasticity and viscosity. *Annu. Rev. Physiol.* 49:209–219.

Ingber, D. E. 1990. Fibronectin controls capillary endothelial cell growth by modulating cell shape. *Proc. Natl. Acad. Sci. USA.* 87:3579–3583.

Ingber, D. E. 1991. Integrins as mechanochemical transducers. *Curr. Opin. Cell Biol.* 3:841–848.

Ingber, D. E. 1993a. The riddle of morphogenesis: a question of solution chemistry or molecular cell engineering? *Cell.* 75:1249–1252.

Ingber, D. E. 1993b. Cellular tensegrity: defining new rules of biological design that govern the cytoskeleton. *J. Cell Sci.* 104:613–627.

Ingber, D. E., and J. Folkman. 1989. Mechanochemical switching between growth and differentiation during fibroblast growth factor-stimulated angiogenesis in vitro: role of extracellular matrix. *J. Cell Biol.* 109:317–330.

Ingber, D. E., J. A. Madri, and J. D. Jamieson. 1981. Role of basal lamina in the neoplastic disorganization of tissue architecture. *Proc. Natl. Acad. Sci. USA.* 78:3901–3905.

Ingber, D. E., J. A. Madri, and J. D. Jamieson. 1986. Basement membrane as a spatial organizer of polarized epithelia: exogenous basement membrane reorients pancreatic epithelial tumor cells in vitro. *Am. J. Pathol.* 122:129–139.

McMahon, T. A. 1984. Muscles, Reflexes, and Locomotion. Princeton University Press, Princeton, NJ.

Mooney, D., L. Hansen, S. Farmer, J. Vacanti, and D. Ingber. 1992. Switching from differentiation to growth in hepatocytes: control by extracellular matrix. *J. Cell Physiol.* 151:497–505.

Oster, G. 1984. On the crawling of cells. *J. Embryol. Exp. Morph.* 83: 327–364.

Peterson, N. O., W. B. McConnaughey, and E. L. Elson. 1982. Dependence of locally measured cellular deformability on position on the cell, temperature, and cytochalasin B. *Proc. Natl. Acad. Sci. USA.* 79: 5327–5331.

Plopper, G., and D. E. Ingber. 1993. Rapid induction and isolation of focal adhesion complexes. *Biochem. Biophys. Res. Commun.* 193:571–578.

Sims, J., S. Karp, and D. E. Ingber. 1992. Altering the cellular mechanical force balance results in integrated changes in cell, cytoskeletal and nuclear shape. *J. Cell. Sci.* 103:1215–1222.

Stamenovic D. 1990. Micromechanical foundations of pulmonary elasticity. *Physiol. Rev.* 70:1117–1140.

Stossel, T. P. 1993. On the crawling of animal cells. *Science.* 260: 1086–1094.

Valberg, P. A. 1984. Magnetometry of ingested particles in pulmonary macrophages. *Science.* 224:513–516.

Valberg, P. A., and D. F. Albertini. 1985. Cytoplasmic motions, rheology and structure probed by a novel magnetic particle method. *J. Cell Biol.* 101:130–140.

Valberg, P. A., and J. P. Butler. 1987. Magnetic particle motions within living cells: physical theory and techniques. *Biophys. J.* 52:537–550.

Valberg, P. A., and H. A. Feldman. 1987. Magnetic particle motions within living cells: measurements of cytoplasmic viscosity and motile activity. *Biophys. J.* 52:551–561.

Wang, N., J. P. Butler, and D. E. Ingber. 1993. Mechanotransduction across the cell surface and through the cytoskeleton. *Science.* 260:1124–1127.

Zaner, K. S., and P. A. Valberg. 1989. Viscoelasticity of F-actin measured with magnetic microparticles. *J. Cell Biol.* 109:2233–2243.